Biophys Rev (2016) 8:409–427
DOI 10.1007/s12551-016-0218-6

REVIEW

Dynamic light scattering: a practical guide and applications in biomedical sciences

Jörg Stetefeld[1,2] · **Sean A. McKenna**[1,2] · **Trushar R. Patel**[3,4]

Received: 13 June 2016 / Accepted: 8 September 2016 / Published online: 6 October 2016

Abstract Dynamic light scattering (DLS), also known as photon correlation spectroscopy (PCS), is a very powerful tool for studying the diffusion behaviour of macromolecules in solution. The diffusion coefficient, and hence the hydrodynamic radii calculated from it, depends on the size and shape of macromolecules. In this review, we provide evidence of the usefulness of DLS to study the homogeneity of proteins, nucleic acids, and complexes of protein–protein or protein–nucleic acid preparations, as well as to study protein–small molecule interactions. Further, we provide examples of DLS's application both as a complementary method to analytical ultracentrifugation studies and as a screening tool to validate solution scattering models using determined hydrodynamic radii.

Keywords Analytical ultracentrifuge · Diffusion coefficient · Dynamic light scattering · Hydrodynamic radius · Light scattering · Protein–ligand interactions · Protein–nucleic acid complexes · Protein–protein complexes

This article is part of a Special Issue on 'Analytical Quantitative Relations in Biochemistry' edited by Damien Hall and Stephen Harding.

✉ Jörg Stetefeld
jorg.stetefeld@ad.umanitoba.ca

✉ Trushar R. Patel
trushar.patel@uleth.ca

[1] Department of Chemistry, University of Manitoba, 144 Dysart Road, Winnipeg, Manitoba R3T 2N2, Canada

[2] Department of Biochemistry and Medical Genetics, University of Manitoba, 745 Bannatyne Avenue - Basic Medical Sciences Building, Winnipeg, Manitoba R3E 0J9, Canada

[3] School of Biosciences, University of Birmingham, Edgbaston, Birmingham B15 2TT, UK

[4] Alberta RNA Research and Training Institute, Department of Chemistry & Biochemistry, University of Lethbridge, 4401 University Drive, Lethbridge, Alberta T1K 3M4, Canada

Introduction

Detection of light scattering from matter is a useful technique with applications in numerous scientific disciplines where, depending on the light source and detector, specific properties of molecules can be studied. In a typical light-scattering experiment, sample is exposed to a monochromatic wave of light and an appropriate detector detects the signal. One of the earliest light-scattering experiments was described by John Tyndall, which characterized light scattering from colloidal suspensions (Tyndall effect), where particles are larger than the wavelength of the incident light (Tyndall 1868). Soon after, Lord Rayleigh described light scattering from particles that are smaller than the wavelength of light (Rayleigh scattering), which explained both that the sky's blue colour is a result of scattering of light due to atmospheric particles and that the refractive index of the scattering medium plays a crucial role in light scattering (Strutt 1871a, b). In contrast to Rayleigh theory, Gustav Mie (1908) described a theory (Mie theory) to study the scattering of light from absorbing and non-absorbing particles that are large compared to the wavelength of light by taking into account particle shape and the difference in refractive index between particles and the medium the particles are present in. Peter Debye suggested that scattering for particles can be studied independently of assumptions on mass, size, or shape as a function of angle (Debye 1915), which is often referred as Rayleigh–Debye scattering.

The usefulness of light scattering as a method to characterize the diffusion behaviour of particles in solution resulted from a series of seminal discoveries. Einstein and

Smoluchowski proposed that liquid should be considered as a continuous medium where thermal fluctuations create inhomogeneities, which result in density and concentration fluctuations (Fluctuation theory of light scattering, Einstein (1910); v. Smoluchowski 1908). Einstein (1905) also established Brownian motion theory (named after Robert Brown) explaining molecular motion of particles. He established that particles were subjected to random forces due to constant collision with solvent molecules resulting in random walk of particles, and that the mean squared displacement of particles due to Brownian motion is proportional to time. Later, Einstein also established a relationship between the diffusion coefficient of particles to their translational friction by including the discovery from Sir George Stokes (1845) that suggested that the friction exerted by a moving particle is proportional to its radius and to the viscosity of the solvent surrounding particles (Einstein 1906). At the same time, William Sutherland also presented a very similar derivation of the Stokes–Einstein equation independently (Sutherland 1905). However, until this point the role of optical anisotropy on angular dependence, intensity, and polarization of scattered light had not been studied. Cabannes and Rocard (1929) and Gans (1921; 1923) addressed the theory of optically anisotropic scatters as well as their influence on polarisation of scattered light. By this time the Rayleigh–Gans–Debye (RGD) theory was established that included scattering from large particles; however, Zimm's (1945; 1948) modifications to RGD equations led the foundation of modern light-scattering approaches that are being utilized to determine size, shape, and molecular weight of macromolecules in solution. On the other hand, Leon Brillouin (1914; 1922) proposed formation of two peaks in the frequency distribution of scattered light caused by the scattering of light by phonons (quasi-particles of sound), resulting in two peaks in the Rayleigh (central) line in the frequency spectrum which was later named as the Brillouin doublet. This phenomenon was further evaluated by Gross (1930) and Landau and Placzek (1934), which in conjunction with the development of laser optics in the 1960s would revolutionize the light-scattering studies of molecules in liquids. Pecora (1964) established that the diffusion of macromolecules in solution led to broadening of the frequency profile of scattered light. Pike and co-workers developed the first digital autocorrelator in 1969 and performed experiments on haemocyanin to determine its diffusion coefficient (Foord et al. 1970). Thus, the relationship between light scattering and diffusion behaviour of particles was established and experimentally verified, which eventually allowed characterization of molecules in solution using light-scattering methods. These events are briefly summarised in Table 1.

Over the years, Pecora, Cummins, Pike and others (Bloomfield and Lim 1978; Cummins et al. 1964; Fujime 1972; Jakeman and Pike 1969; Pecora 1972; Pike 1972) had developed various approaches to determine the diffusion coefficient of molecules in solution, and ultimately their contributions led to the development of the modern dynamic light-scattering (DLS) instrument, with Malvern Instruments (Malvern, UK) commercializing the first modern DLS instruments followed by Brookhaven (Long Island, USA) and ALV (Langen, Germany). Since its inception, DLS has proven particularly popular in determining hydrodynamic behavior of proteins, nucleic acids, and viruses due to its ability to provide information on both size and aggregation. There are already a number of excellent reviews detailing the theory and applications of DLS (Bloomfield 1981; Fujime 1972; Harding and Jumel 1998; Harvey 1973; Jamieson et al. 1972; Lorber et al. 2012; Nieuwenhuysen and Clauwaert 1981; Nobbmann et al. 2007; Rimai et al. 1970; Schurr 1977; Serdyuk et al. 2007; Van Holde 1970; Zakharov and Scheffold 2009). Here, our aim is to provide a brief theoretical background, an update on applications of DLS in studying proteins, nucleic acids, and their complexes, and a discussion of the benefits that modern instruments offer.

Theoretical considerations

When a monochromatic beam of light encounters solution containing macromolecules, light scatters in all directions as a function of the size and shape of the macromolecules. In static light scattering, the intensity of scattered light is analysed as time-averaged intensity, which provides useful information on molecular weight and radius of gyration of macromolecules. On the other hand, if the intensity fluctuations (caused due to Brownian motion of macromolecules in solution) of scattered light is analysed, the diffusion coefficient (D_τ) that is related to hydrodynamic size of macromolecules can be obtained. Dynamic light scattering, also known as photon correlation spectroscopy or quasi-elastic light scattering, is a technique that primarily measures the Brownian motion of macromolecules in solution that arises due to bombardment from solvent molecules, and relates this motion to the size (or D_τ) of particles. Such motion of macromolecules depends on their size, temperature, and solvent viscosity (Harding and Jumel 1998). Therefore, knowledge of accurate temperature is essential for DLS measurements, since the viscosity of solvent depends on the temperature (Harding 1999). When the movement of particles over a time range is monitored, information on the size of macromolecules can be obtained, as large particles diffuse slowly, resulting in similar positions at different time points, compared to small particles (such as solvent molecules) which move faster and therefore do not adopt a specific position.

In a dynamic light-scattering instrument, when laser light encounters macromolecules the incident light scatters in all directions and scattering intensity is recorded by a detector. The monochromatic incident light will undergo a phenomenon called Doppler broadening as the macromolecules are in continuous motion in solution (Harding and Jumel 1998). The

Table 1 Timeline of major events

Historical developments	References
Friction experienced by moving particles is related to its radius and solvent viscosity	Stokes (1845)
Tyndall effect: light scattering from colloidal suspensions	Tyndall (1868)
Rayleigh scattering: blue colour of sky due to the scattering of light by atmospheric particles, importance of refractive index in light scattering	Strutt (1871a; 1871b)
Mie scattering: scattering of light from particles larger than the wavelength of light	Mie (1908)
Brownian motion theory: collision with solvent molecules results in random motion of particles	Einstein (1905)
Stokes–Einstein relationship: combines light scattering and diffusion behaviour of particles	Einstein (1906), Sutherland (1905)
Fluctuation theory of light scattering: thermal fluctuations result into local inhomogeneities and intensity of scattered light can be determined by the mean-square fluctuations in density and/or concentration	Einstein (1910), v. Smoluchowski (1908)
Rayleigh–Debye scattering: particles can be studied without assumptions on mass, size or shape as a function of angle	Debye (1915)
Theory of optically anisotropic scatters	Cabannes and Rocard (1929), Gans (1921; 1923)
Brillouin doublet: theory and verification	Brillouin (1914; 1922), Gross (1930), Landau and Placzek (1934)
Siegert relation: relationship between the electric field correlation and intensity correlation function	Siegert (1949)
Beginning of the modern light scattering approaches	Pecora (1964)
Digital autocorrelator development and diffusion coefficient measurement of haemocyanin	Foord et al. (1970)
Cumulant analysis method for monomodal systems	Koppel (1972)
Exponential sampling method	Ostrowsky et al. (1981)
Constrained regularization method for inverting data	Provencher (1982a; 1982b)
Non-negative least squares analysis method	Morrison et al. (1985)
Maximum-entropy method	Livesey et al. (1986) Nyeo and Chu (1989)
Singular value and reconstruction method	Finsy et al. (1992; 1989)

scattered light will either result in mutually destructive phases and cancel each other out, or in mutually constructive phases to produce a detectable signal. The digital autocorrelator then correlates intensity fluctuations of scattered light with respect to time (ns-μs) to determine how rapidly the intensity fluctuates, which is related to the diffusion behaviour of macromolecules. In a dynamic light-scattering experiment, we measure the $G_2(\tau)$, an intensity correlation function (or second-order correlation function) that describes the motion of macromolecules under investigation and can be expressed as an integral over the product of intensities at time t and delayed time $(t + \tau)$ (Berne and Pecora 1976):

$$G_2(\tau) = \langle I(t)I(t+\tau)\rangle \tag{1}$$

where, τ is the lag time between the two time-points.

The $G_2(\tau)$ can be normalised as:

$$g_2(\tau) = \frac{\langle I(t)I(t+\tau)\rangle}{\langle I(t)\rangle^2} \tag{2}$$

The braces in both equations represent averaging of properties over the duration of the experiment (time t).

In a typical light-scattering experiment, it is not possible to precisely know how each particle moves in solution; however, the motion of particles relative to each other is correlated by means of an electric field correlation function, $G_1(\tau)$, also known as the first-order correlation function, which illustrates correlated particle movement and can be defined as:

$$G_1(\tau) = \langle E(t)E(t+\tau)\rangle \tag{3}$$

where, $E(t)$ and $E(t+\tau)$ represent the scattered electric fields at times (t) and $(t + \tau)$

Similarly to equation 2, an equation 3 can be normalized as:

$$g_1(\tau) = \frac{\langle E(t)E(t+\tau)\rangle}{\langle E(t)E(t)\rangle} \tag{4}$$

The $g_1(\tau)$ and $g_2(\tau)$ can be coupled to each other by the Siegert relation (1949) based on an approximation that the scattering is *homodyne* (photodetector detects only

scattered light) and that the photon counting is a random Gaussian process,

$$g_2(\tau) = B + \beta|g_1(\tau)|^2 \quad (5)$$

where, B is the baseline (~1) and β is the coherence factor that depends on detector area, optical alignment, and scattering properties of macromolecules.

For monodisperse particles, the electric field correlation factor, $g_1(\tau)$ decays exponentially and is dependent on a decay constant, Γ, for macromolecules undergoing a Brownian motion.

$$g_1(\tau) = e^{-\Gamma\tau} \quad (6)$$

Therefore, equation 5 can be rewritten as:

$$g_2(\tau) = 1 + \beta e^{-2\Gamma\tau} \quad (7)$$

However, for a polydisperse system, $g_1(\tau)$ cannot be represented as a single exponential decay but as an intensity-weighed integral over a distribution of decay rates G(Γ) represented as:

$$g_1(\tau) = \int_0^\infty G(\Gamma)e^{-\Gamma_\tau d\Gamma} \quad (8)$$

The decay constant, Γ in equation 6 is directly related to the diffusion behaviour of macromolecules (D_τ) as expressed in the following equation.

$$\Gamma = -D_\tau q^2 \quad (9)$$

In Equation 9, the Bragg wave vector q is proportional to solvent refractive index n (Harding 1999).

$$q = \frac{4\pi\eta}{\lambda} sin(\theta/2) \quad (10)$$

Where, λ is the wavelength of incident light and, θ is angle at which the detector is placed.

Therefore, equation 7 can be rewritten as:

$$g_2(\tau) = 1 + \beta e^{-2D_\tau q^2 \tau} \quad (11)$$

Thus, equation 11 connects the particle motion with the measured fluctuations (Burchard 1983).

DLS instruments employ either a detector at 90 ° (e.g., DynaPro® NanoStar® from Wyatt Technology or Zetasizer Nano S90® from Malvern Instruments) or a backscatter detection system at 173 ° (e.g., Zetasizer Nano S® from Malvern Instruments) and at 158 ° (DynaPro Plate Reader® from Malvern Instruments) close to the incident light of 180 °. Compared to the detection at 90 °, at a high scattering angle, the contributions of rotational diffusion effects in the observed autocorrelation profiles can be neglected and the D_τ can be obtained (Harding 1999; Pusey 1972). As light does not travel through the entire sample in the cuvette, the backscattering detection system also allows for measurement of the D_τ of highly concentrated samples since multiple scattering phenomenon (scattering of a photon by more than one particles in contrast to scattering of a photon by only one particle) of scattered light can be avoided. Furthermore, large dust particles and contaminants scatter more light in the forward direction as their scattering becomes wavelength-independent compared to smaller size particles (Rayleigh scattering) that have nearly equal scattering in both directions, scattering contribution of large particles could be avoided in a backscatter detecting system.

As the translational diffusion coefficient, D_τ, is concentration-dependent, it should be measured at multiple concentrations and extrapolated to infinite dilution (D^0_τ) as a standard practice. Furthermore, the D^0_τ can be converted to the standard solvent conditions (viscosity and temperature of water at 20 °C) to obtain $D^0_{\tau,20,w}$ (Harding and Jumel 1998; Raltson 1993). The D_τ is extremely useful in the determination of other important hydrodynamic parameters. For example, the hydrodynamic radius (R_h), which can be defined as the radius of a hypothetical sphere that diffuses at the same rate as particle under investigation, can be obtained using the Stokes–Einstein equation (Pusey 1972).

$$D_\tau = \frac{k_B T}{6\pi\eta R_h} \quad (12)$$

Where k_B is Boltzmann coefficient (1.380×10^{-23} $kg.m^2.s^{-2}.K^{-1}$), T is an absolute temperature, and η is the viscosity of medium.

Additionally, the translational frictional coefficient, f (F/v, ratio of frictional force F experienced by moving particles due to Brownian motion and the velocity v of the particle) that provides information on the shape of macromolecules can also be calculated using D_τ by the following equation.

$$f = \frac{RT}{N_A D_t} \quad (13)$$

Where R is a gas constant (8.314×10^{-7} erg/mol.K), T is an absolute temperature, and N_A is Avogadro's number (6.022137×10^{23} mol).

The frictional coefficient can also be calculated using R_h and equation (12) (Tanford 1961).

$$f = 6\pi\eta R_h \quad (14)$$

The translational frictional coefficient can be further used along with the D_τ to calculate frictional ratio (f/f_0, ratio of Stokes radius to that of a sphere with the volume of an unsolvated macromolecule) of macromolecules that can provide information with regard to the solution conformation of

macromolecules. For a compact sphere, the frictional ratio is unity and as the shape of macromolecules deviate from compact sphere, f/f_0 increases.

Data analysis

Modern instruments are supplied with packages that perform data analysis, using various approaches to primarily evaluate size and homogeneity of macromolecules. In this section, we provide the background in brief on data analysis strategies. The correlation function (equation 11) contains information on diffusion behaviour of macromolecules under investigation, which in turn has information on R_h (equation 12). In order to gain reliable information on diffusion coefficient, primarily two approaches are used to fit the correlation function – monomodal distribution and nonmonomodal distribution methods.

Monomodal distribution — cumulant analysis

The cumulant analysis method, also known as the method that does not require a priori information, provides mean values of the diffusion coefficient but not the distribution of diffusion coefficients. Therefore, this method is only suitable for Gaussian-like distributions around the mean values. As explained in equation 6, the electric field correlation factor, $g_1(\tau)$ decays exponentially and is dependent on a decay constant, $\Gamma(\Gamma = -D_\tau q^2)$. For a monodisperse system, the g_1 (τ) can be treated as a single exponential decay function to calculate the decay constant and hence the diffusion coefficient. However, often the experimental system is polydisperse, which requires the $g_1(\tau)$ to be treated as the sum of several exponential decay functions that decays at different rates.

The cumulant analysis method was introduced by Koppel (1972) which became widely popular due to its ease and reliability, and was considered as the method of choice by the International Standards Organisation (ISO) in 1996 and again in 2008 (ISO 2008). Other methods including singular value and reconstruction methods were also developed, however, they are not as popular for the data analysis (Finsy et al. 1989, 1992). Koppel (1972) derived the cumulative-generating function $K(-\tau, \Gamma)$ that is related to the logarithm of $g_1(\tau)$ and the m^{th} cumulant of distribution function $k_m(\Gamma)$:

$$k_m(\Gamma) = \frac{d^m K(-\tau,\Gamma)^m}{d(-\tau)}\Bigg|-\tau = 0 \text{ where, } K(-\tau,\Gamma) = ln g_1(\tau) \quad (15)$$

The $k_m(\Gamma)$ can be rewritten to derive moments about the mean (μ_m):

$$\mu_m = \int_0^\infty G(\Gamma)(\Gamma-\bar{\Gamma})^m d\Gamma \quad (16)$$

as

$$k_1(\tau) = \int_0^\infty G(\Gamma)\Gamma d\Gamma = \bar{\Gamma},\ k_2(\tau) = \mu_2,\ k_3(\tau) = \mu_3,\ k_4(\tau) = \mu_4 - 3\mu_2^2 \ldots \quad (17)$$

where, $\overline{\Gamma}$ is the mean of Γ values. Here, based on the Taylor expansion of $K(-\tau, \Gamma)$ about $(\tau) = 0$, the $\ln g_1(\tau)$ (see, equation 15) can be rewritten as:

$$K(-\tau,\Gamma) = ln g_1(\tau) = -\bar{\Gamma}\tau + \frac{k_2}{2!}\tau^2 - \frac{k_3}{3!}\tau^3 + \frac{k_4}{4!}\tau^4 \ldots \quad (18)$$

If we now recall equation 5, [Siegert relation (1949)] and convert it to a logarithmic mode, we can obtain,

$$ln(g_2(\tau) - B) = ln\beta + 2 ln g_1(\tau) \quad (19)$$

Finally, by combining equations 18 and 19, we can obtain:

$$ln(g_2(\tau) - B) = ln\beta + 2\left(-\bar{\Gamma}\tau + \frac{k_2}{2!}\tau^2 - \frac{k_3}{3!}\tau^3 + \frac{k_4}{4!}\tau^4 \ldots\right) \quad (20)$$

Equation 20 has some useful properties. First of all, the experimentally measured and normalized $g_2(\tau)$ could be plotted against (τ) to fit the parameters on the right-hand side of the equation. The $\bar{\Gamma}$ (k_1), k_2, k_3 and k_4 represents average, variance, skewness and kurtosis of measured distributions respectively for the decay rates of the Gaussian distribution. More importantly, the polydispersity index (PDI) could be derived by using $k_2/\ \bar{\Gamma}^2$ relationship. Ideally, parameters above k_3 are not used to prevent over fitting of the data. It should be noted that often data truncation is required (typically when the autocorrelation function decays ~ 10 % of the maximum value) because as the signal decays into the baseline, the higher noise could drive signal to negative values which are not useful as the data processing requires mathematical treatment of data such as square root and logarithm. Also, random errors lead to huge variations fitting of cumulants. For example, with the highly sophisticated instruments, random errors in $\bar{\Gamma}$ could be as low as 1 % but for k_2 it could be as high as 20 %. Therefore, the high-order cumulants are not recommended to be used (Koppel 1972).

Non-monomodal distribution methods

Unlike the cumulant analysis, non-monomodal methods do not assume a certain type of distribution of diffusion properties, and are more suitable for polydisperse systems. The *non-negative least squares* (NNLS) method was developed by Morrison et al. (1985) for broad monomodal or multimodal distributions, which involves non-negativity constraints and the geometrical spacing of the distribution based on the Laplace transform of equation 8. The NNLS method uses decay constants $\bar{\Gamma}$ representing decay rates $G(\Gamma)$ spaced in a linear or logarithmic form over a chosen ranges of Γ. For Γ_i, the b_i coefficients can be obtained from the best fit to the data with in the NNLS constraints using following equation.

$$\chi^2 = \sum_{j=1}^{N} \left[g_1(\tau_j) - \sum_{i=1}^{M} b_i e^{(-\Gamma_i \tau_j)} \right]^2 \tag{21}$$

Where N is the number of data points and M is the number of decay constants with the constraint that Γ_i, and b_i are zero or positive values (Hassan and Kulshreshtha 2006).

The main drawback of NNLS is its sensitivity to small variations in measurements (of both, data and errors). To address this issue, the maximum-entropy (Livesey et al. 1986) method was developed, which was subsequently modified to include geometrical spacing (Nyeo and Chu 1989).

Another inversion method that utilizes restraints to specify the range and values of a set of Γ_i, before data processing, to obtain a unique set of parameters for a reliable fit, is known as the *exponential sampling* method where, Γ_i values are exponentially spaced (Ostrowsky et al. 1981):

$$\Gamma_{i+1} = \Gamma_i e^{(\eta\pi/\omega_{max})} \tag{22}$$

where, $\omega_{\max}$ is the maximum possible value of ω determined by the experimental noise that does not involve negative values for b_i in equation 21. It is calculated through a trial and error method by gradually increasing ω until negative values for the distribution coefficients are obtained. Since each Γ is related to the R_h (equations 9, 10 and 12), a frequency histogram of the radius distribution can be obtained using this method.

The *constrained regularization method for inverting data* (CONTIN) that also involves Laplase transform was developed by Provencher (1982a; 1982b; with Stepanek 1996) and is one of the most popular data analysis methods that does not involve sequential optimization of $\omega_{\max}$ like the *exponential sampling* method. The CONTIN technique uses a modified version of NNLS equation that includes minimization of *regularised* residuals (unlike minimization of residuals in the NNLS equation) and an appropriate weighing function. Therefore, a modified expression of equation 21 can be written as:

$$\chi^2 = \sum_{j=1}^{N} \left(1/\sigma_i^2\right) \left[g_1(\tau_j) - \int G(\Gamma) e^{(-\Gamma\tau)} d\Gamma \right]^2 + \alpha^2 \| LG(\Gamma) \|^2 \tag{23}$$

Here, α is a regularizer that adds an additional constraint on the solution while performing data analysis, whereas L is the operator of regularizer.

The CONTIN method employs a nonlinear statistical technique to smooth the solution, a regularizer parameter based on the F-test and a parsimony principle that chooses distribution function with the least detailed distribution that agrees with the data, resulting in narrower distributions. The major discoveries in data analysis are briefly summarised in Table 1.

Although the DLS measures the PDI (cumulant analysis, $k_2/\bar{\Gamma}^2$, Equation 20), it should not be compared with the PDI measured by the static light-scattering method (ratio of weight–average molar mass to number–average molar mass, M_w/M_n) as based on the $k_2/\bar{\Gamma}^2$ ratio, PDI from DLS is in the range of 0–1, where in theory, a value of zero represents a monodisperse system, whereas that for M_w/M_n would be ~1. Typically, the cumulant analysis method is suitable for samples with the PDI of ~0.1, i.e., monodisperse system. The PDI value of 0.1 to 0.7 represents nearly monodisperse preparation, whereas PDI >0.7 suggests broad distribution of macromolecular sizes in solution and non-monomodal distribution methods should be considered for data analysis. PDI of < 0.05 is rarely observed in biological systems.

Size distribution of hydrodynamic radius

The methods described in sections 3.1 and 3.2 will provide distribution of diffusion behaviour, and hence the distribution of R_h. The averaged diffusion coefficient ($\langle D_\tau \rangle$) in a given system can be expressed as:

$$\langle D_\tau \rangle = \frac{\sum_i N_i M_{w,i}^2 P(q,R) D_{\tau i}}{\sum_i N_i M_{w,i}^2 P(q,R)} \tag{24}$$

where M_w is the molecular weight of N number of particles, and $P(q,R)$ is the intraparticle interface.

Equation 24 describes the dependence of the diffusion coefficient on M_w^2, which explains that the technique is inherently biased for molecules with higher molecular weights. It should also be noted that the scattering of light depends on the refractive index of macromolecules, and that the term $P(q,R)$ can be approximated to 1 for molecules sufficiently smaller than the wavelength of the incident light, resulting in z-averaged D_τ. Since it is the intensity fluctuations of

macromolecules that are being collected and analysed in a DLS experiment, the first-hand information on R_h is based on the *intensity-weighted distribution* or simply, *intensity distribution* that provides z-average R_h. As light scattering depends on the refractive index of macromolecules and solvent viscosity, the z-averaged R_h requires input of these two properties. According to the Rayleigh approximation, the intensity distribution is approximately proportional to (size)^6 for small particles (Barnett 1942), as presented in equation 25. It should be noted that the z-averaged R_h from DLS should only be compared with R_h from other methods if the molecules under investigation are monodisperse and display monomodal distribution, particles are spherical in shape, and are solubilized in suitable buffer system, as the intensity distribution depends on the refractive index of molecules and viscosity of the medium.

$$\%I_a = \frac{a^6 N_a.100}{N_a a^6 + N_b b^6} \tag{25}$$

Equation 25 describes intensity distribution for a solution containing N_a and N_b molecules with size a and b respectively. The $\%I_a$ presents intensity-weighted distribution for particles with size a, based on the relative amount of intensity of molecules with size a (Malvern 2014).

The *intensity-weighted distribution* can be converted to *volume-weighted distribution* that represents relative proportion of multiple sizes in a particular sample based on their volume or size but not their intensity, by taking advantage of the Mie theory. According to the Rayleigh approximation, the mass of spherical molecules is proportional to (size)^3. If the density of a system is uniform, mass can be approximated to the volume, implying that the volume-weighted distribution is proportional to (size)^3, which is why the R_h from volume distribution is smaller compared to *intensity-weighted distribution*.

$$\%V_a = \frac{a^3 N_a.100}{N_a a^3 + N_b b^3} \tag{26}$$

Equation 26 describes volume distribution for a solution containing N_a and N_b molecules with size a and b respectively. The $\%V_a$ presents volume-weighted distribution for molecules with size a, based on the volume of molecules with size a.

In addition to the knowledge of refractive index and viscosity, volume distribution relies on the assumption that all the molecules are homogenous and spherical in shape, and that the intensity distribution has no errors. Because volume distribution presents distribution of sizes based on volume/mass of molecules, it is practically more useful.

The intensity-weighted distributions can also be converted to *number-weighted distributions* that represent number of molecules in each bin in a given histogram. Equation 27 presents number distribution for a system containing two molecules.

$$\%N_a = \frac{N_a.100}{N_a + N_b} \tag{27}$$

Where, N_a and N_b are molecules with size a and b respectively. The $\%N_a$ presents number-weighted distribution for molecules with size a based on the number of molecules with size a.

Standard operating protocol

We have used a Zetasizer Nano S from Malvern Instruments Ltd. to perform all the experiments described here with low-volume quartz cuvette ZEN2112 from Hellma Analytics. However, the approach could be modified to suit any equivalent modern DLS instrument.

Cuvette cleaning

For efficient cleaning, it is recommended to use a dedicated cuvette washer (e.g., C1295 from Sigma–Aldrich).

- Wash cuvette with approximately 5 ml of 5 % solution of Hellmanex™ from Hellma Analytics or similar detergent solution.
- Wash cuvette with approximately 5 ml of 5 % acetic acid solution (ACS grade).
- Wash cuvette with approximately 10 ml of ultrapure water (e.g., Type 1 quality water from Milipore Milli-Q systems).
- Dry cuvette with approximately 5 ml of 70 % ethanol. Keep cuvette for additional 5 minutes on the cuvette washer to allow sufficient drying.
- Dust particles scatter light that may affect the DLS measurements. A standard check is then performed to ensure sufficient cleaning using only filtered buffer in the cuvette, where an error (e.g., insufficient counts to obtain reliable results) results indicating that the cuvette is clean and contains no particles that can interfere with measurements.

Analysing biomolecular preparations to detect aggregation

We refer to preparations containing proteins, glycoproteins, nucleic acids (RNA, DNA), protein–protein complexes (PPC) or protein–nucleic acids complexes (PNC) as biomolecular preparations. It is important to note that samples subjected to DLS analysis are "polished samples" and not "crude preparations" meaning that the proteins, nucleic acids, or their

complexes have been already purified by means of various forms of chromatography [e.g., affinity chromatography, ion-exchange chromatography, hydrophobic interaction chromatography, and/or size exclusion chromatography (SEC)] to achieve a high level of purity. One of the most important criteria in biomedical sciences is ensuring that the biomolecular preparation is devoid of high molecular weight aggregates (HMWA), as aggregation can be a major rate-limiting factor in biochemical, biophysical, and biopharmaceutical studies. For example, an aggregated and/or inhomogeneous sample will be difficult to crystallise — an essential step to obtain a high-resolution structure by X-ray crystallography. Several biophysical techniques such as small-angle X-ray scattering (SAXS) and small angel neutron scattering (SANS) can only provide reliable information for monodisperse and homogenous preparations, as molecules with higher molecular weight (albeit at extremely low concentration) will scatter heavily thereby affecting the outcomes of these experiments. As a practical commercial example, therapeutic antibodies need to go through a rigorous analysis that involves investigation of their aggregation state (amongst other properties including temperature, storage stability, and degradation) before the selection of a lead antibody candidate for therapeutic applications.

The following is a standard protocol the authors use in their laboratory for analysis of proteins, antibodies, glycoproteins, nucleic acids, and their complexes for structure biology applications.

- Clean cuvette as described in subsection "Monomodal distribution — cumulant analysis".
- Filter the sample through 0.1 μm filter (e.g., Ultrafree-MC VV Centrifugal Filter, Merck Millipore) to remove large particulates from the preparation.
- It is critical to study aggregation state at the working concentrations (concentrations at which the downstream study is planned, e.g., crystallization or antibody dose). Prior to all measurements, concentration for polished sample should be accurately measured.
- Often, biological samples are precious since they require time and resources. To minimise the sample requirement, we use a cuvette that requires only ~12 μl of filtered concentrated sample. However, to avoid air bubbles we load ~20 μl of sample carefully by reaching the bottom of the cuvette with a straight pipette tip.
- The software package that accompanies modern DLS instruments (such as the Zetasizer Nano S software) enables creation of a standard operating protocol (SOP) for an individual sample. We recommend that for each particular sample, a SOP should be prepared that contains essential information such as the buffer composition and experimental temperature (that in turn will calculate the viscosity at particular temperature and refractive index of buffer: essential parameters for reliable DLS measurements).
- Perform the R_h distribution measurements at least five times to obtain reproducible results at high concentration. In order to study the concentration dependence of R_h, we dilute the preparation by directly adding filtered buffer into the cuvette containing a high concentration of sample followed by gentle mixing using pipette and collect data. We continue this practice for multiple concentrations.

Often, we use well-characterised proteins such as BSA or ovalbumin as positive controls to ensure that the instrument is performing as expected. In addition, several NIST (National Institute of Standards and Technology) standards such as 60 nm or 100 nm polystyrene latex spheres should also be used to ensure proper instrument function.

The Zetasizer software provides a number of analysis methods to study aggregation by DLS. Size Distribution by Intensity and Size Distribution by Volume are the most widely used methods, whose theories are discussed in the "Data analysis" section, and usefulness in practice is discussed in the next sections. The choice of the analysis method will depend on the objective of study. For example, if an analysis is aimed to study the presence of trace amount of aggregates for lead therapeutic antibody preparation (to achieve aggregation-free preparation), the intensity distribution method is more suitable, as high molecular weight aggregates will disproportionately scatter light relative to smaller particles enabling detection despite their relatively low concentration in the sample. On the other hand, if the study is aimed to investigate homogeneity to set-up crystallization trials or for additional biochemical/biophysical characterisation using analytical ultracentrifuge, SAXS, etc., purity around 95 % is acceptable and the volume distribution method can be used.

Applications

The dynamic light-scattering technique has a number of advantages over other methods. For example, it is possible to conduct experiments with wide range of sample buffer and wide range of temperature as well as concentrations. DLS is also a non-invasive technique that requires comparatively low amounts of sample and provides reliable estimates of the quality of preparation rapidly. In the following sections, we describe applications of DLS to study homogeneity of proteins, RNA, and their complexes.

Detecting aggregation of recombinant proteins

Probing homogeneity of biomolecular preparations is required for various types of downstream experiments and applications. This section focuses on study of a multi-domain extracellular matrix protein (ECM), nidogen-1 (ND-1), and a well-studied globular protein, ovalbumin.

ND-1 (139 kDa) is a key basement membrane protein that primarily interacts with other ECM proteins such as laminin, perlecan, fibulin, and fibronectin (Gerl et al. 1991; Hsieh et al. 1994; Mayer et al. 1993; Sasaki et al. 1995a, b). It is a very difficult system to study, as it undergoes proteolytic degradation as well as aggregation. In order to investigate its low-resolution structure, we required a homogenous preparation devoid of both degradation and aggregation. Initial expression and purification trials produced heterogeneous preparations as presented in Fig. 1a and b; however, subsequent optimization achieved high quality preparations without significant degradation and with less than 5 % of HMWA as detected by intensity distributions (Fig. 1c). It is important to note that in Rayleigh scattering, the scattering intensity depends on the 6th power of the size of molecules (Barnett 1942), and therefore despite being present in negligible amounts, the HMWA R_h peak intensity is disproportionately represented relative to the dominant smaller molecular weight monodisperse species in the same preparation. Therefore, the HMWA peak is absent in the volume distribution (Fig. 1d). This example clearly highlights DLS as a sensitive tool to screen for even trace amounts of HMWA in biomolecule preparations.

Figure 2a presents an intensity distribution profile for ovalbumin (44 kDa) at multiple concentrations, where HMWA (>100 nm) are visible for each concentration. However, the volume distribution profiles derived from the intensity information for each concentration display a single peak, since the amount of aggregates is negligible (Fig. 2b). As a volume distribution profile represents the relative volume of high and low molecular weight species in a preparation (discussed in section 3.3), we will mainly focus on the volume distribution profiles in subsequent sections. Ideally, to report R_h value, it should be first measured multiple times at each individual concentration followed by calculating mean R_h value at each concentration and plotting against concentration to eliminate concentration effects, similar to the approach taken with diffusion and sedimentation coefficient measurements. We have provided an example here with ovalbumin (Fig. 2c), a practice that is routinely followed in our approach for proteins and nucleic acids as well as PPC and PNC to obtain a reliable

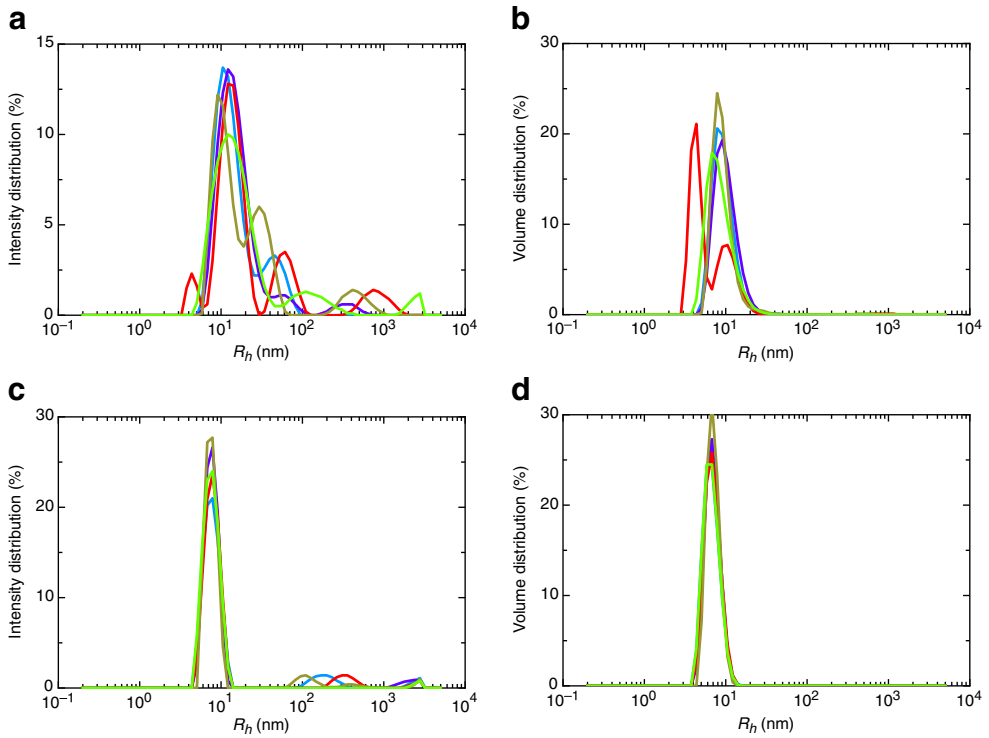

Fig. 1 Evaluating homogeneity of protein solution. **a** Hydrodynamic radius distribution by intensity for nidogen-1 (ND-1) at 0.4 mg/ml, indicating that although there is a major peak for each measurement, there are multiple peaks visible between 15 nm and 500 nm (*x*-axis) suggesting the presence of high molecular weight aggregated species. Degradation at 4 nm is also visible for one of the measurements in *red* colour. **b** Hydrodynamic radius distribution by volume derived from intensity profiles for ND-1 at 0.4 mg/ml concentration, suggesting that volume distribution is not sensitive enough for detecting scant amount of aggregation. However, peaks from multiple runs do not coincide with each other: that essentially is a reflection of heterogeneous sample. Again, the degradation is visible for the measurement that is clearly visible for intensity distribution. **c** Similar to **a**, the aggregation studies for ND-1 were performed at 0.5 mg/m for a preparation optimized to obtain cleaner sample, indicating that compared to **a**, the level of aggregation is severely reduced. **d** Homogeneity of ND-1 reflected by volume distribution of nearly identical peaks from multiple measurements, demonstrating highly purified and homogenous preparation. Recombinant ND-1 (139 kDa) was expressed into 293-EBNA cells and purified using affinity chromatography, followed by SEC in 50 mM Tris–HCl (pH 7.5), 200 mM NaCl buffer as described earlier (Patel et al. 2014)

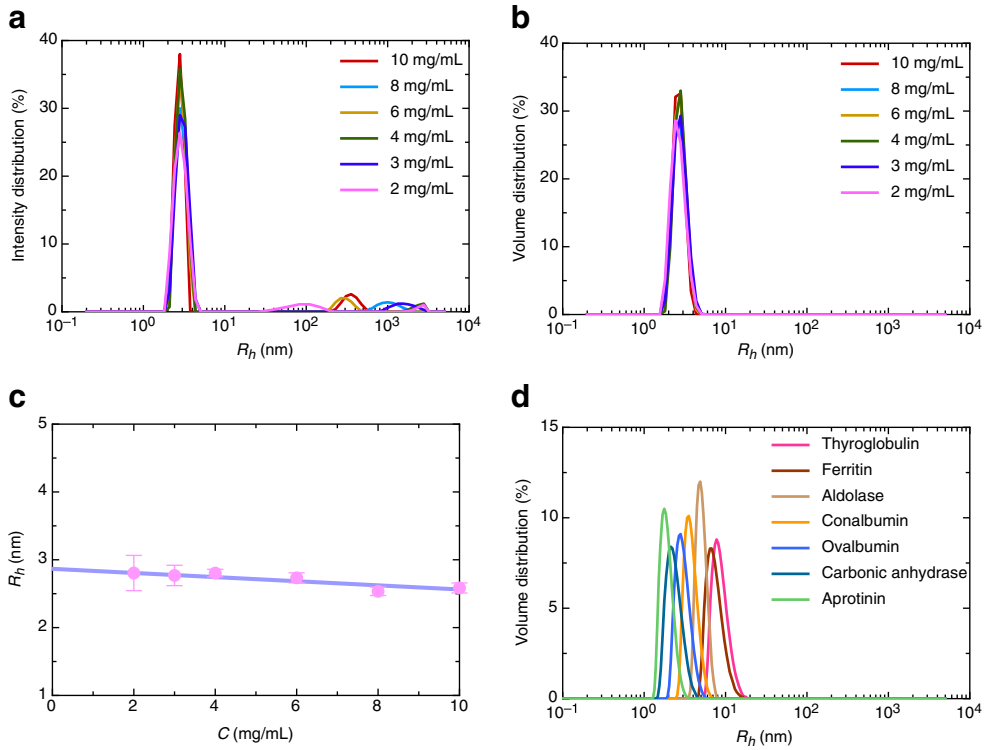

Fig. 2 Homogeneity studies of ovalbumin. **a** and **b** represents R_h distribution at multiples concentrations for ovalbumin. The intensity distributions (**a**) suggest presence of ~5 % aggregated material at 100 nm and above. Those peaks are not present in volume distribution profiles (**b**) since the amount of aggregated material is negligible. However, since large molecules scatter light more strongly, even a trace amount of aggregation can be detected using intensity distribution. In both cases, nearly identical positions of peak suggest a homogenous preparation. For biophysical and structure biology applications, such preparations are acceptable; however, for therapeutic antibodies, further optimization may be required. **c** Plot of R_h vs concentration for ovalbulin, where the *y*-axis intercept provides concentration-independent R_h of 2.88 ± 0.06 nm. **d** Hydrodynamic radius for frequently used molecular weight standards to calibrate size exclusion column was measured at single concentration. The details for molecular weights and concentrations are provided in Table 2. Note that all of the proteins used here are globular proteins; therefore, it is possible to compare their R_h profiles in terms of molecular weight. The smallest protein here is aprotinin (*Mw* 6.5 kDa) with R_h of 1.82 nm, a value that increases with increase in molecular weight to 8.71 nm for thyroglobulin (*Mw* 670 kDa). Ovalbumin (44 kDa) was purchased from Fischer Scientific (BP2535) and solubilised using 20 mM phosphate buffer (pH 7.0) for DLS measurements (Scott et al. 2011). The molecular weight standards kit was purchased from GE healthcare, and DLS data were collected in 50 mM Tris (pH 8.0), 150 mM NaCl buffer

estimate of R_h. In addition to ovalbumin, we also evaluated routinely used molecular weight standards that are globular in shape at a single concentration to evaluate resolution of DLS measurements (Table 2). Fig. 2d presents gradual increase in R_h from 1.82 nm for aprotinin with M_w of 6.5 kDa to 8.71 nm for thyroglobulin with M_w of 670 nm, suggesting that it is possible to study macromolecules with a wide range of molecular weights.

Protein–protein interaction studies

In addition to detection of aggregation in biomolecular preparations, DLS can also be employed to study PPC. Ideally, the SEC-purified proteins are first studied by DLS alone, followed by analysis of the complex by DLS after SEC purification. An example of PPC studies using DLS is provided in Fig. 3a and b, which presents DLS data for ND-1 (139 kDa), LM γ−1 (109 kDa), and their complex. LM γ−1, an interacting partner of ND-1 and Net4, plays crucial roles in basement membrane formation (Breitkreutz et al. 2004; Schneiders et al. 2007) cell migration, and metastasis (Kuratomi et al. 2002). Single nucleotide polymorphisms in LM γ−1 gene is linked with premature ovarian failure (Pyun et al. 2012). Figure 3a presents the R_h distribution data for SEC purified ND-1 and LM γ−1 proteins at single concentration. After studying how individual proteins behave at multiple concentrations in terms of their homogeneity by DLS, we also investigated their complex using DLS (Fig. 3a). The R_h distribution studied at multiple concentrations suggested that both proteins are highly monodisperse in solution, with R_h of 6.80 ± 0.10 nm and 6.40 ± 0.05 nm respectively (Fig. 3b). Furthermore, the complex of ND-1 - LM γ−1 was also found to be monodisperse with R_h of 9.00 ± 0.04 nm (Fig. 3b). This example clearly demonstrates the strengths of DLS technique — very rapid measurements and requiring low amounts of purified components to study protein–protein interactions.

Table 2 Hydrodynamic radius of routinely used globular proteins

Protein	M_w (kDa)	*Conc.* (g/l)	R_h (nm)*
Thyroglobulin	670	2	8.71 ± 0.21
Ferritin	440	3	7.17 ± 0.24
Aldolase	158	4	4.98 ± 0.08
Conalbumin	75	5	3.72 ± 0.08
Ovalbumin	44	5	2.98 ± 0.04
Carbonic anhydrase	29	6	2.37 ± 0.05
Aprotinin	6.5	8	1.82 ± 0.05

* Determined at a single concentration in 50 mM Tris, 150 mM NaCl at pH 8.0

Homogeneity of viral RNA molecules

RNA molecules are highly labile, since exposure to trace amounts of ribonuclease impurities present in aqueous solutions and reagents, air and dust particles, as well as direct human skin contact with RNA preparations, can result in RNA degradation. Our dynamic light-scattering instrument is regularly used to study homogeneity of in-vitro transcribed RNA. The West Nile virus genome terminal regions (5' and 3') are recognised by an enzyme called 2' 5' oligoadenylate synthetase 1 (OAS1), which is a part of an innate immune system. Once viral RNA is recognised, OAS1 synthesises 2'-5'-linked oligoadenylates that ultimately stimulate RNase L in order to slow viral propagation (Hovanessian and Justesen 2007). We studied interactions of the 5' terminal region (5' TR) with OAS1 as well as 3' terminal region (3' TR) using a variety of biochemical and biophysical tools, one of which was DLS. While interpreting DLS data for RNA molecules, it should be noted that the folded RNA structures are typically extended; therefore, the R_h of RNA is often observed to be higher compared to a globular protein of similar molecular weight. This effect has been observed qualitatively by SEC (Kim et al. 2007). Figures 4a and b present a monodisperse preparation of the West Nile virus 5' TR based on intensity and volume distributions respectively at 3.5 mg/ml, whereas Fig. 4c and d presents intensity and volume distributions for 3' TR from West Nile virus at 2.7 mg/ml. Both distributions for each sample suggest that the 5' TR and 3' TR RNA are free of any aggregation and suitable for low-resolution shape determination using SAXS. The DLS data for 5' TR (47.5 kDa) and 3' TR (37.5 kDa) were calculated at multiple concentrations to obtain R_h of 5.1 ± 0.02 nm and 3.46 ± 0.06 nm respectively compared to ovalbumin, a globular protein with M_w of 44 kDa that has R_h of ~3 nm, suggesting that both of these RNA has an extended structure in solution, which was later confirmed by low-resolution solution scattering studies (Deo et al. 2014, 2015). These examples clearly establish DLS as an ideal method to study homogeneity and conformation of RNA molecules prepared in laboratory using in-vitro transcription.

Protein–RNA interaction studies

As with PPC studies, protein–RNA complexes can also be studied using DLS. We have used DLS to characterise OAS1–RNA complex and PKR–RNA complexes. In order to study the homogeneity of complexes, it is ideal to simultaneously study individual components. Therefore, host OAS1 (41 kDa) protein, 5' TR RNA as well as 3' TR RNA from West Nile virus were studied at multiple concentrations. As mentioned above, Fig. 4 displays homogeneity of 5' TR and 3' TR, whereas Fig. 5a presents DLS data for OAS1 demonstrating monodispersity of OAS1. Additionally, the purity of 5' TR-OAS1 complex and 3' TR-OAS1 complex is also evident from Fig. 5a. The complexes (5' TR–OAS1 and 3' TR–OAS1) were also studied at multiple concentrations, similarly to OAS1, 5' TR, and 3' TR. The DLS data for individual components and complex suggest that all the species are highly pure in solution. The R_h values obtained from

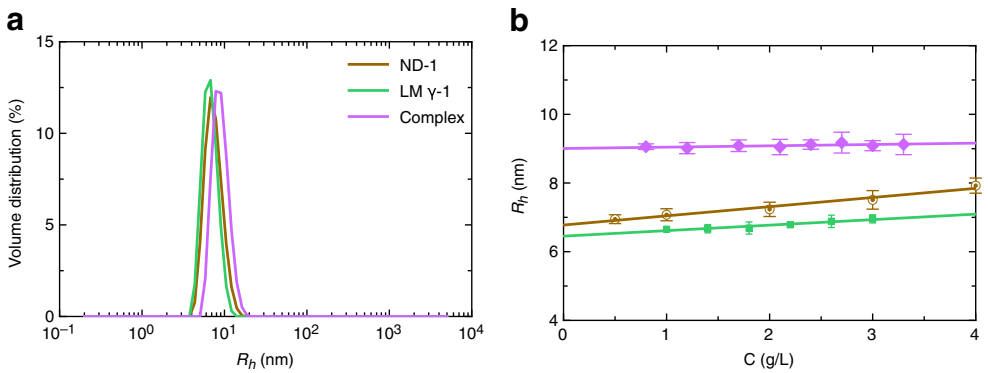

Fig. 3 Homogeneity of protein-protein complexes. **a** Hydrodynamic radius distribution of ND-1, laminin γ-1 (LM γ−1) arm, and their complex at 3 mg/ml indicating purity of individual species as well as their complex. **b** Concentration dependence of ND-1, LM γ−1 arm, and their complex up to 4 mg/ml (Patel et al. 2014). Recombinant ND-1 (139 kDa) and LM γ-1 (109 kDa) were expressed into 293-EBNA cells and purified using affinity chromatography followed by SEC. Complex of ND-1-LM γ-1 was purified using SEC, and DLS measurements were performed in 50 mM Tris–HCl (pH 7.5), 200 mM NaCl buffer as described earlier (Patel et al. 2014)

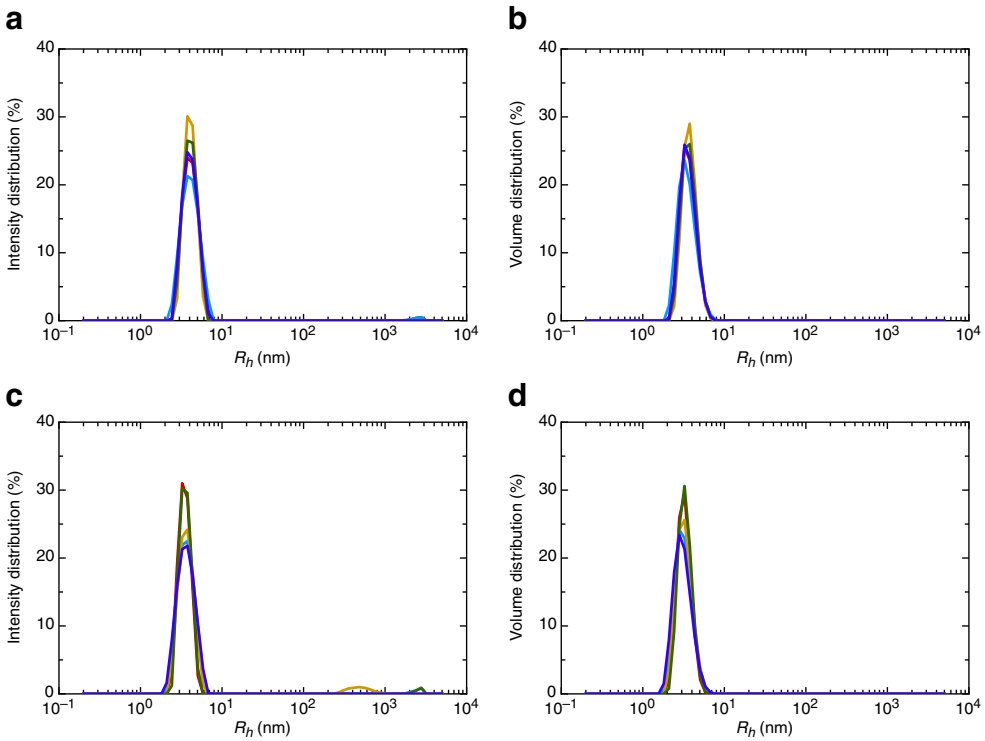

Fig. 4 Evaluating homogeneity of viral RNA preparations. Multiple measurements for intensity distribution (**a**) and volume distribution (**b**) at 3.5 mg/ml suggest that the 5' TR RNA is highly pure and devoid of any aggregation. Similarly, 3' untranslated region (3' TR) from West Nile virus was also studied using DLS at 2.7 mg/ml, where **a** and **b** present intensity and volume distributions suggesting presence of a homogenous solution of 3' TR. The 5' and 3' untranslated regions (5' TR — 47.5 kDa, 3' TR — 37.5 kDa) from West Nile virus were prepared using an in-vitro transcription method followed by purification using SEC and DLS analysis in 50 mM Tris (pH 7.0), 100 mM NaCl buffer as described earlier (Deo et al. 2014, 2015)

multiple concentrations are: OAS1 (3.30 ± 0.3 nm), 5' TR (5.10 ± 0.2 nm), 3' TR (3.36 ± 0.06 nm), 5' TR–OAS1 (4.92 ± 0.07) and 3' TR–OAS1 (5.45 ± 0.03). OAS1 is a globular-shaped protein (Deo et al. 2014; Donovan et al. 2013), whereas both RNA molecules were found to be extended in solution. Isothermal titration calorimetry studies for both complexes established 1:1 ration of individual species (Deo et al. 2014, 2015); therefore, a decrease of R_h for 5' TR–OAS1 complex and an increase of R_h in 3' TR–OAS1 complex clearly indicate conformational change in RNA molecules. Overall, both examples suggest that DLS, in conjunction with other methods, can be employed to study conformational changes mediated by interacting partners in solution.

PKR is a major player of innate immunity providing support against viral infection by recognising viral double-stranded RNA, and ultimately influences a number of cellular activities (Garcia et al. 2006). It is composed of two double-stranded RNA binding motifs (dsRBM) connected by a flexible linker as well as a kinase domain that is linked to dsRBMs by a linker (Dzananovic et al. 2014; McKenna et al. 2007). In order to study the low-resolution structure of double-stranded RNA binding domain of PKR ($PKR_{1–169}$, 18.8 kDa) in complex with adenovirus VA_I RNA that lacks the terminal region ($VA_I\Delta TS$, 32.2 kDa), DLS was employed as a tool to study homogeneity of $PKR_{1–169}$, $VA_I\Delta TS$ and their complex. The homogeneity of each species and the complex is evident from Fig. 5c, that essentially has a single peak for each sample without any HMWA. The DLS data were collected at multiple concentrations and extrapolated to infinite dilution to obtain R_h of 2.80 ± 0.10 nm for $PKR_{1–169}$, 3.30 ± 0.04 nm for $VA_I\Delta TS$ and 3.90 ± 0.2 nm for their complex (Dzananovic et al. 2014). This example suggests that as above, DLS can be a powerful tool to study homogeneity of proteins, RNA, and their complexes. As described in Section 5.6, these R_h values can also used to validate low-resolution structures or individual components and complexes.

Protein–small molecules interactions

Agrin is a heparin sulphate proteoglycan located in the extracellular matrix, and plays a crucial role in aggregation of neuromuscular junction (Nitkin et al. 1987) and formation of synapses (Hilgenberg et al. 2006; Hoover et al. 2003; Khan et al. 2001). It is composed of an N-terminal domain (NtA), a series of follistatin-like domains (FS), and three laminin G-like C-terminal domains (G1, G2, and G3) (Mascarenhas et al. 2003; Stetefeld et al. 2001). The C-terminal G3 domain of agrin is known to interact with calcium if the alternative amino-acid splicing site has eight amino-acid inserts present (Stetefeld et al. 2004). However, we attempted to investigate if the G3 domain without any amino acid present at the splice site can interact with divalent cations. It should be noted that the G3 domain was expressed as a fusion protein that contains Fc domain of human IgG (G_3B_0Fc), which facilitates purification by means of protein A affinity chromatography. For each measurement, 20 μl of G_3B_0Fc (~1 mg/ml) protein was added to a clean cuvette and allowed to equilibrate to 20 °C for 5 minutes followed by measurement of R_h.

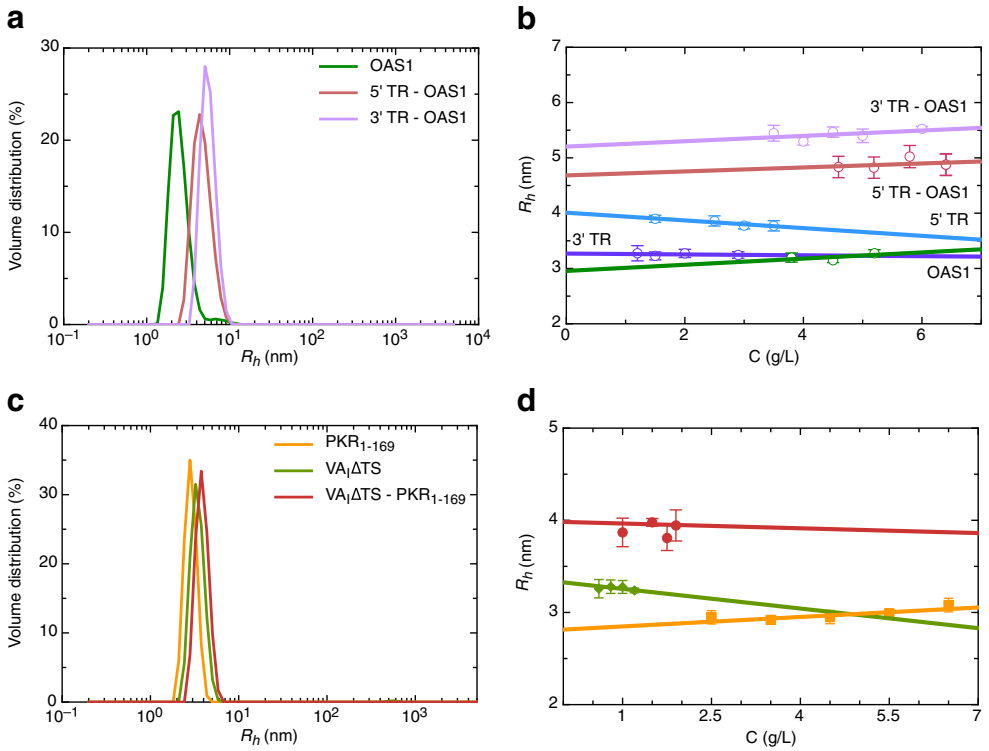

Fig. 5 Homogeneity of protein-RNA complexes. **a** Homogeneity studies of OAS1 (2.2 mg/ml), 5' TR–OAS1 complex (4.0 mg/ml), and 3' TR–OAS1 complex (3.5 mg/ml). **b** The concentration dependence of OAS1, 5' TR, 3' TR, 5' TR - OAS1, and 3' TR–OAS1 complex. **c** Hydrodynamic radius distribution for $PKR_{1–169}$ (3.5 mg/ml), $VA_I\Delta TS$ (1.2 mg/ml), and $VA_I\Delta TS$–$PKR_{1–169}$ complex (1 mg/ml), suggesting homogeneity of all three species. **d** Dynamic light scattering data for $PKR_{1–169}$, $VA_I\Delta TS$, and $VA_I\Delta TS$–$PKR_{1–169}$ complex are presented at multiple concentrations. Human OAS1 (41 kDa) was expressed in BL21(DE3) cells followed by purification by means of affinity and SEC (Meng et al. 2012). DLS data were measured in 50 mM Tris (pH 7.5), 100 mM NaCl, 1 mM DTT buffer (Deo et al. 2014). The 5' TR–OAS1 and 3'–TR OAS1 complexes were purified using SEC and analysed using DLS in 50 mM Tris (pH 7.5), 40 mM NaCl, and 1 mM EDTA (Deo et al. 2015). Similarly, the adenovirus VA_I RNA lacking the terminal stem-loop RNA ($VA_I\Delta TS$, 32.3 kDa) was prepared by in-vitro transcription method followed by purification using SEC (Dzananovic et al. 2014), whereas human protein kinase R (PKR) lacking the C-terminal kinase domain ($PKR_{1–169}$ 18.8 kDa) was expressed into BL21(DE3) cells, purified by means of affinity and SEC followed by DLS data collection in 50 mM Tris (pH 7.50), 100 mM NaCl, and 5 mM 2-mercaptoethanol (Dzananovic et al. 2013). DLS data for SEC purified $VAI\Delta TS$–$PKR_{1–169}$ complex was collected in 50 mM Tris (pH 7.50), 100 mM NaCl buffer (Dzananovic et al. 2014)

As presented in Fig. 6 for each set of experiments, an R_h of ~ 5 nm was observed for G_3B_0Fc that corresponds to a monomer as deduced from AUC and DLS experiments (Patel et al. 2011). After measuring the R_h for $G_3B_0F_c$ protein, $CaCl_2$ was added into the cuvette to final concentration of 5 mM followed by temperature equilibrium/incubation for 5 minutes prior to measurement of R_h to determine effect of $CaCl_2$ on protein. The procedure was repeated to increase $CaCl_2$ concentration up to 50 mM. Figure 6a demonstrates the effect of $CaCl_2$, where addition of 5 mM $CaCl_2$ led to formation of a supramolecular complex of G_3B_0Fc yielding two peaks (major peak ~ 600 nm) that increased to ~ 800 nm when $CaCl_2$ concentration was increased to 50 mM. Since EDTA binds to divalent cations, we then added EDTA to final concentration of 5 mM into the cuvette containing G_3B_0Fc protein with 50 mM $CaCl_2$. After 5 minutes of temperature equilibrium of sample, the DLS measurements were performed, which yielded a peak at ~ 5 nm for G_3B_0Fc that is nearly identical to the first measurement where $CaCl_2$ was absent. Similarly, experiments were performed to study effect of $MnCl_2$ and $ZnCl_2$ where the R_h for G_3B_0Fc was measured first followed by addition to $MnCl_2$ or $ZnCl_2$ to final concentration of only 2 mM, which resulted into supramolecular complex with peak ~ 900 nm which could be reduced to the original size of G_3B_0Fc upon addition of EDTA to final concentration of 5 mM, as presented in Fig. 6b and c. We also performed similar experiments with $MgCl_2$; however, only marginal increase in R_h for G_3B_0Fc was observed at 50 mM $MgCl_2$ concentration (data not shown). These results demonstrate that the G_3 domain of agrin can interact with metal ions resulting into reversible aggregates of various sizes depending on the metal ion. However, if such behaviour of G_3 domain of agrin in vitro has any biological relevance remains to be demonstrated. It could be argued that the presence of Fc domain may influence such behaviour of agrin G_3 protein; however, we were unable to find such effect of cations on antibodies in

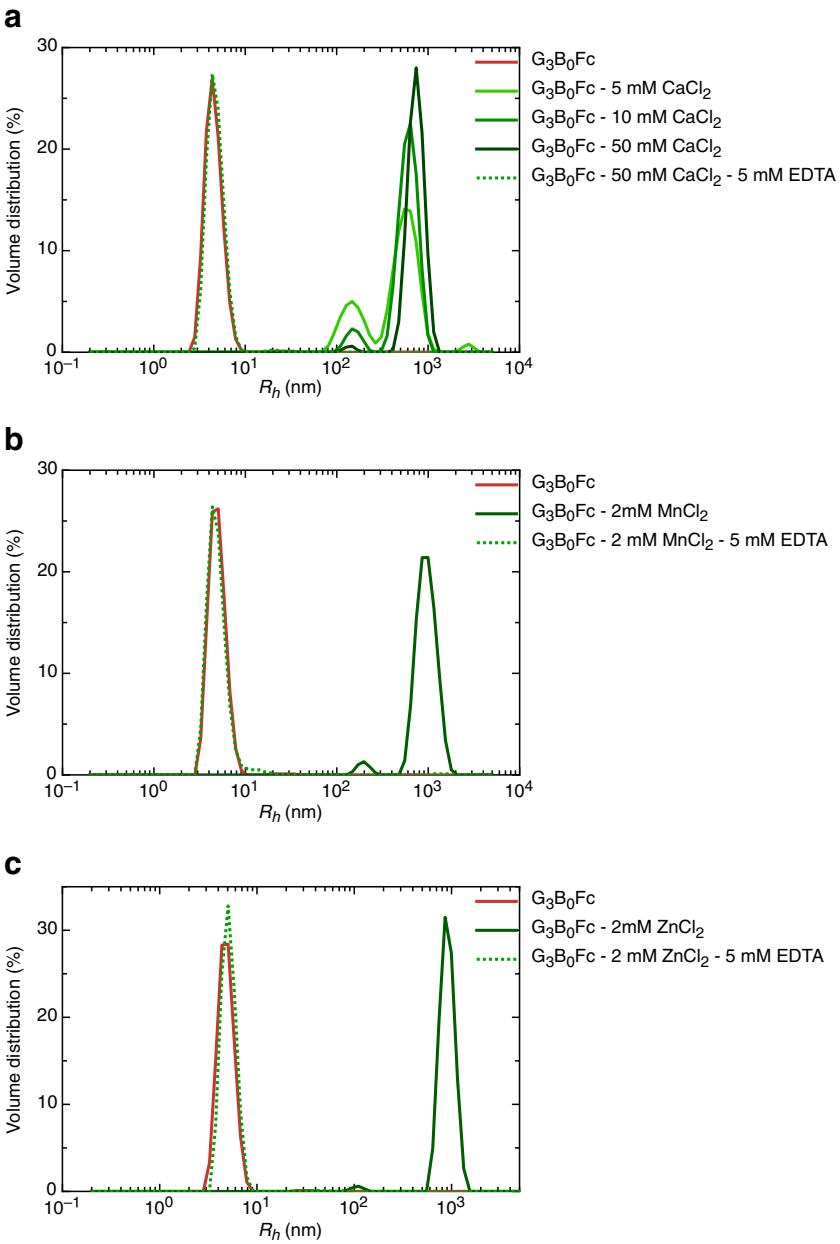

Fig. 6 Protein–small molecules interaction studies. The mouse G_3B_0 protein fused with human Fc domain of IgG–G_3B_0Fc was studied using DLS at 1 mg/ml. **a**, **b**, and **c** presents volume distribution profiles for G_3B_0Fc protein and its interactions with divalent cations. **a** A single peak for G_3B_0Fc appears at ~5 nm which resolves into two peaks at ~ 100 nm and ~ 600 nm upon addition of 5 mM $CaCl_2$. The higher molecular weight peak further increases up to ~ 700 nm in the presence of 50 mM $CaCl_2$. However, addition of EDTA (5 mM) reduces the huge complex of G_3B_0Fc–50 mM CaCl2 to ~ 5 nm that essentially overlays on G_3B_0Fc data. Similarly, addition of only 2 mM $MnCl_2$ (**b**) and 2 mM $ZnCl_2$ (**c**) increases the size of G_3B_0Fc from ~ 5 nm to ~900 nm, indicating presence of a very heavy aggregate. Addition of EDTA (5 mM in both cases) again reduces the heavy complex to monomeric size of G_3B_0Fc. The C-terminal laminin G-like G_3 domain variant of chicken agrin without insert of amino acids at the alternative splice site B (B_0), G_3B_0 was expressed as a fusion protein, with human Fc domain of IgG–G_3B_0Fc being expressed using HEK293 cells as described previously (Patel et al. 2011). The G_3B_0Fc protein was affinity purified, followed by DLS data collection in 20 mM Tris, 150 mM NaCl at pH 7.2

the literature. Nevertheless, our data shows that it is possible to study aggregation of macromolecules induced by small molecules using DLS.

Complementary hydrodynamic methods enhanced by DLS measurements

Apart from providing information on homogeneity, DLS can also be employed as a complementary method to study size and shape of macromolecules. In this section, we will provide a brief outline of applications of DLS as a complementary method.

Molecular weight determination

Molecular weight is one of the most important properties of any molecule. Comparison of sequence molecular weight of proteins or nucleic acids with experimentally determined molecular weight can provide useful information such as their oligomeric status, degradation, or change in molecular weight upon interaction between binding partners. There are a number of methods that can provide molecular weight information. For example, SEC can, in theory provide molecular weight for proteins, nucleic acids, or complexes. However, the molecular weight calculated from SEC relies on the assumption that the molecular weight standard and biomolecules being studied

adopt a spherical shape; deviations in shape typically result in overestimates of molecular weight from elongated structures. A more reliable method for calculating molecular weight is to combine sedimentation coefficient data from an analytical ultracentrifuge and R_h from the dynamic light scattering using the Svedberg equation (Svedberg and Pedersen 1940),

$$M_w = \frac{6\pi\eta_0 R_h N_A s^0_{20,w}}{1-\nu\bar{\rho}_0} \quad (28)$$

where, $\bar{\nu}$ is the partial specific volume, η_o is the solvent viscosity and ρ_o is the solvent density.

Previously, we have used such an approach to determine molecular weights of proteins — laminin γ-1 arm, G_3 domain of agrin fused with human IgG Fc, N-terminal domain of RHAU, and OAS1, as well as VA_I RNA (Deo et al. 2014; Dzananovic et al. 2014; Meier et al. 2013; Patel et al. 2010, 2011). Thus, R_h information from DLS can be a very useful parameter when combined with the sedimentation coefficient to obtain molecular weight information.

Homogeneity studies of biological samples exposed to high-energy X-rays

SAXS is a type of static light-scattering technique that utilizes X-rays to allow determination of low-resolution shape of macromolecules in solution. SAXS data can either be collected at the synchrotron using high-energy X-rays or from in-house sources where the X-rays source is much weaker. Typically, in-house SAXS data collection (~20 °C) requires 2–4 hours of sample exposure time to X-rays, compared to the synchrotron source that requires only a few seconds. Furthermore, while collecting SAXS data, the user normally collects data for multiple samples in a single experimental setup starting from buffer, meaning that it could take over 10 hours for some samples. Therefore, samples susceptible to either storage at ~20 °C for extended periods or radiation damage may alter the homogenous preparation of macromolecules to degraded and/or aggregated states. We routinely use DLS to determine sample homogeneity of samples after SAXS data collection of protein, RNA, and their complexes (Deo et al. 2014, 2015; Dzananovic et al. 2013, 2014; Meier et al. 2013; Patel et al. 2014).

Furthermore, DLS measurements are an extremely useful independent crosscheck used to validate ab-initio shape reconstruction of macromolecules using SAXS data, a heavily computational process. To validate SAXS models without any bias, we calculate hydrodynamic parameters including R_h and sedimentation coefficient from the models using program HYDROPRO (Ortega et al. 2011b), and compare them to experimentally determined properties by DLS and complementary hydrodynamic techniques. It is also possible to study DNA and polysaccharides using packages in the HYDRO family (Amoros et al. 2011; Benitez et al. 2015). We have followed such practice for proteins, RNA, DNA, and their complexes (Ariyo et al. 2015; Deo et al. 2014, 2015; Dzananovic et al. 2013, 2014; Meier et al. 2013; Patel et al. 2010, 2011, 2012, 2014; Vadlamani et al. 2015).

Shape analysis in combination with radius of gyration

The radius of gyration (R_g) parameter, defined as an average root mean squared distance from the centre of the mass of a macromolecule, can be obtained using static light-scattering studies where the intensity of scattered light is analysed. For proteins and nucleic acids, SAXS or SANS methods are employed to measure R_g. The ratio of R_g to R_h could provide indication of conformation of macromolecules in solution. For globular proteins the ration is ~ 0.70, and it increases as the shape changes from globular to extended rigid particles (Burchard 1992). Table 3 summarises the R_g and R_h values of some of the proteins and RNA we have studied previously, with their R_g/R_h ratios. We have used SAXS data to construct low-resolution structures of these macromolecules, which essentially validated our preliminary shape information of these macromolecules. Thus, the DLS can be used in conjunction with static light scattering to deduce shape information.

In order to obtain more reliable and unbiased information on shape (flexible coil, rods, cylinders, spheres) of macromolecules (DNA, RNA, polysaccharides, proteins, and viruses), Garcia de la Torre and colleagues (Amoros et al. 2011; Ortega and Garcia de la Torre 2007) developed a different concept where instead of using R_h and R_g as well as their ratios, a variation of those properties and their ratios were implemented. For example, instead of using R_h or D_r, equivalent radii, T that is related to diffusion properties ($T = f/6\pi\eta_0$) can be used. Similarly, for R_g, equivalent radii, G ($\sqrt{5/3}R_g$) can be used, which in turn could be utilised to obtain G/T, which is a very useful ratio indicating solution conformation of macromolecules (Ortega et al. 2011a; Ortega and Garcia de la Torre 2007). Typically, the ration of G/T is ~1 for spherical particles and >1 for elongated macromolecules (Table 3).

Limitations

Although DLS is a highly useful method as discussed above, it suffers the following disadvantages:

(i) DLS measurements are very sensitive to temperature and solvent viscosity. Therefore, the temperature must be kept constant and solvent viscosity must be known for a reliable DLS experiment.
(ii) DLS is a low-resolution method that often cannot separate molecules that are closely related (e.g., monomer and dimer).

Table 3 Combination of radius of gyration and hydrodynamic radius provides shape information

Samples	R_g (nm)	R_h (nm)	R_g/R_h	G/T	Shape	Reference
ND-1	7.20 ± 0.10	6.80 ± 0.10	1.06	1.36	elongated	Patel et al. 2014
OAS1	2.28 ± 0.02	3.0 ± 0.03	0.76	0.98	globular	Deo et al. 2014
$RHAU_{53–105}$	2.1 ± 0.20	1.90 ± 0.03	1.10	1.41	elongated	Meier et al. 2013
$PKR_{1–169}$	2.53 ± 0.04	2.80 ± 0.01	0.90	1.16	elongated	Dzananovic et al. 2013
3' TR	4.15 ± 0.03	3.46 ± 0.06	1.12	1.44	elongated	Deo et al. 2015
5' TR	5.10 ± 0.02	5.10 ± 0.01	1.00	1.29	elongated	Deo et al. 2014
HIV-1 TAR RNA	2.60 ± 0.05	2.70 ± 0.02	0.96	1.23	elongated	Dzananovic et al. 2013
Adenovirus VA_I RNA	4.35 ± 0.07	3.8 ± 0.04	1.14	1.47	elongated	Deo et al. 2015
Adenovirus $VA_I\Delta TS$	3.71 ± 0.06	3.30 ± 0.04	1.12	1.44	elongated	Dzananovic et al. 2014
Adenovirus VA_IAS	2.45 ± 0.02	2.58 ± 0.05	0.95	1.22	elongated	Dzananovic et al. 2013
hTR1-20 RNA quadruplex	1.31 ± 0.08	1.91 ± 0.02	0.68	0.87	disk-shaped	Meier et al. 2013
Q2 RNA quadruplex	1.62 ± 0.01	2.01 ± 0.025	0.81	1.04	disk-shaped	Ariyo et al. 2015

(iii) Although it is possible to measure the molecular weight using DLS where intensity of scattered light [K^*c/R_θ, where K* is an optical parameter, c is concentration and R_θ is an angular dependent light-scattering parameter, also known as the Rayleigh ratio; see Wyatt (1993) for more details] is plotted against concentration, it is not a very reliable and reproducible method. In such cases, alternate methods such as static light scattering coupled with multiangle laser light scattering and analytical ultracentrifuge should be used.

(iv) DLS is also restricted to transparent sample preparation.

(v) As the scattering intensity depends on the 6th power of the size of macromolecules (I proportional d^6 where d is a diameter of macromolecule), large aggregates — even a very small amount will affect the measurements. Therefore, the sample-holding cuvette must be cleaned thoroughly and sample must be filtered prior to DLS measurements.

(*vi*) The signal from DLS depends on the size and concentration of macromolecules. Therefore, to obtain reliable measurements, optimization of range of concentration may be required.

Conclusions

In this review, we have provided a brief historical and theoretical background on DLS. The examples for homogeneity and interaction studies of proteins, nucleic acids, and their complexes using a highly versatile DLS method are also presented. Although it suffers from minor limitations as discussed in section 6, it is gaining popularity in academic and industrial laboratories. DLS is a non-invasive method that provides fast, precise, and reproducible quality check to study aggregation in biomolecular preparation requiring very little amounts of sample.

Acknowledgments TRP acknowledges Manitoba Institute of Child Health (2008–10) and Canadian Institutes of Health Research (2010–12) for postdoctoral fellowship awards, and Marie Skłodowska-Curie Fellowship program (2013–15) for their financial support. JS holds a Canada Research Chair in Structure Biology and was supported by funding from NSERC. SAM is supported by NSERC Discovery grant (RGPIN-2015-06142). The authors congratulate Prof. Donald Winzor on his 80th birthday and thank him for his immense contributions in the development and applications of biophysical methods. Dr. Patel thanks Prof. Winzor for being his mentor. The authors thank Drs. Hall and Harding for an opportunity to contribute in a special issue "Analytical Quantitative Relations in Biochemistry".

Compliance with ethical standards

Conflict of Interests Jörg Stetefeld declares that he has no conflicts of interest. Sean A. McKenna declares that he has no conflicts of interest. Trushar R. Patel declares that he has no conflicts of interest.

Ethical approval This article does not contain any studies with human participants or animals performed by any of the authors.

References

Amoros D, Ortega A, de la Torre JG (2011) Hydrodynamic properties of wormlike macromolecules: Monte Carlo simulation and global analysis of experimental data. Macromolecules 44:5788–5797. doi:10.1021/ma102697q

Ariyo EO et al (2015) Biophysical Characterization of G-Quadruplex Recognition in the PITX1 mRNA by the Specificity Domain of the Helicase RHAU. PLoS One 10:e0144510. doi:10.1371/journal.pone.0144510

Barnett CE (1942) Some applications of wave-length turbidimetry in the infrared. J Phys Chem 46:69–75. doi:10.1021/j150415a009

Benitez AA, Hernandez Cifre JG, Diaz Banos FG, de la Torre JG (2015). Prediction of solution properties and dynamics of RNAs by means of Brownian dynamics simulation of coarse-grained models: Ribosomal 5S RNA and phenylalanine transfer RNA. BMC Biophys 8:11 doi:10.1186/s13628-015-0025-7

Berne BJ, Pecora R (1976) Dynamic light scattering: with applications to chemistry, biology, and physics. John Wiley & Sons, Inc, New York, USA

Bloomfield VA (1981) Quasi-elastic light scattering applications in biochemistry and biology. Annu Rev Biophys Bioeng 10:421–450. doi:10.1146/annurev.bb.10.060181.002225

Bloomfield VA, Lim TK (1978) Quasi-elastic laser light scattering. Methods Enzymol 48:415–494

Breitkreutz D et al (2004) Inhibition of basement membrane formation by a nidogen-binding laminin gamma1-chain fragment in human skin-organotypic cocultures. J Cell Sci 117:2611–2622. doi:10.1242/jcs.01127

Brillouin L (1914) Light diffusion by a homogeneous transparent body. Cr Hebd Acad Sci 158:1331–1334

Brillouin L (1922) Diffusion de la lumière et des rayons X par un corps transparent homogène, influence de l'agitation thermique. Annales de Physique (Paris) 17:88–122

Burchard W (1983) Static and dynamic light scattering from branched polymers and biopolymers. In: Light scattering from polymers. Springer, Berlin Heidelberg, pp 1–124. doi:10.1007/3-540-12030-0_1

Burchard W (1992) Static and dynamic light scattering approaches to structure determination of biopolymers. In: Harding SE, Settele DB, Bloomfield VA (eds) Laser light scattering in biochemistry. Royal Society of Chemistry, Cambridge, pp 3–22

Cabannes J, Rocard Y (1929) La diffusion moléculaire de la lumière, Vol 16 of Recueil des conférences-rapports de documentation sur la physique. Les Presses Universitaires de France

Cummins HZ, Knable N, Yeh Y (1964) Observation of diffusion broadening of Rayleigh scattered light. Phys Rev Lett 12:150–153

Debye P (1915). Zerstreuung von Röntgenstrahlen. Annalen der Physik 351:809–823 doi:10.1002/andp.19153510606

Deo S et al (2015) Characterization of the termini of the West Nile virus genome and their interactions with the small isoform of the 2′ 5′-oligoadenylate synthetase family. J Struct Biol 190:236–249. doi:10.1016/j.jsb.2015.04.005

Deo S et al (2014) Activation of 2′ 5′-oligoadenylate synthetase by stem loops at the 5′-end of the West Nile virus genome. PLoS One 9: e92545. doi:10.1371/journal.pone.0092545

Donovan J, Dufner M, Korennykh A (2013) Structural basis for cytosolic double-stranded RNA surveillance by human oligoadenylate synthetase 1. Proc Natl Acad Sci U S A 110:1652–1657. doi:10.1073/pnas.1218528110

Dzananovic E et al (2014) Solution conformation of adenovirus virus associated RNA-I and its interaction with PKR. J Struct Biol 185: 48–57. doi:10.1016/j.jsb.2013.11.007

Dzananovic E, Patel TR, Deo S, McEleney K, Stetefeld J, McKenna SA (2013).Recognition of viral RNA stem-loops by the tandem double-stranded RNA binding domains of PKR. RNA 19:333–344 doi:10.1261/rna.035931.112

Einstein A (1905) Über einen die Erzeugung und Verwandlung des Lichtes betreffenden heuristischen Gesichtspunkt. Annalen Der Physik 322:132–148. doi:10.1002/andp.19053220607

Einstein A (1906). Zur Theorie der Brownschen Bewegung. Annalen Der Physik 324:371–381 doi:10.1002/andp.19063240208

Einstein A (1910) Theory of opalescence of homogenous liquids and liquid mixtures near critical conditions. Annalen Der Physik 33: 1275–1298

Finsy R, Degroen P, Deriemaeker L, Gelade E, Joosten J (1992). Data Analysis of Multi-Angle Photon Correlation measurements without and with prior knowledge. Part Part Syst Char 9:237–251 doi:10.1002/ppsc.19920090133

Finsy R, Degroen P, Deriemaeker L, Vanlaethem M (1989) Singular value analysis and reconstruction of photon correlation data equidistant in time. J Chem Phys 91:7374–7383. doi:10.1063/1.457260

Foord R, Jakeman E, Oliver CJ, Pike ER, Blagrove RJ, Wood E, Peacocke AR (1970) Determination of diffusion coefficients of haemocyanin at low concentration by intensity fluctuation spectroscopy of scattered laser light. Nature 227:242. doi:10.1038/227242a0

Fujime S (1972) Quasi-elastic scattering of laser light. A new tool for the dynamic study of biological macromolecules. Adv Biophys 3:1–43

Gans R (1921) Asymmetry of gas molecules — an article to determine the molecular form. Annalen Der Physik 65:97–123

Gans R (1923) The Tyndall effect in liquids. Z Phys 17:353–397. doi:10.1007/bf01328695

Garcia MA, Gil J, Ventoso I, Guerra S, Domingo E, Rivas C, Esteban M (2006) Impact of protein kinase PKR in cell biology: from antiviral to antiproliferative action. Microbiol Mol Biol Rev 70:1032–1060. doi:10.1128/MMBR.00027-06

Gerl M, Mann K, Aumailley M, Timpl R (1991) Localization of a major nidogen-binding site to domain III of laminin B2 chain. Eur J Biochem 202:167–174

Gross E (1930) Change of wave-length of light due to elastic heat waves at scattering in liquids. Nature 126:201–202. doi:10.1038/126201a0

Harding SE (1999) Protein hydrodynamics. In: Allen G (ed) Protein: a comprehensive treatise, vol 2. JAI Press, Greenwich, CT, pp 271–305

Harding SE, Jumel K (1998) Light scattering. In: Coligan JE, Dunn BM, Ploegh HL, Speicher DW, Wingfield PT (eds) Current protocols in protein science. John Wiley & Sons, Inc., New York. 10.1002/0471140864.ps0708s11

Harvey JD (1973) Diffusion coefficients and hydrodynamic radii of three spherical RNA viruses by laser light scattering. Virology 56:365–368. doi:10.1016/0042-6822(73)90313-9

Hassan PA, Kulshreshtha SK (2006) Modification to the cumulant analysis of polydispersity in quasielastic light scattering data. J Colloid Interf Sci 300:744–748. doi:10.1016/j.jcis.2006.04.013

Hilgenberg LG, Su H, Gu H, O'Dowd DK, Smith MA (2006) Alpha3Na+/K+−ATPase is a neuronal receptor for agrin. Cell 125: 359–369. doi:10.1016/j.cell.2006.01.052

Hoover CL, Hilgenberg LG, Smith MA (2003) The COOH-terminal domain of agrin signals via a synaptic receptor in central nervous system neurons. J Cell Biol 161:923–932. doi:10.1083/jcb.200301013

Hovanessian AG, Justesen J (2007) The human 2′-5′oligoadenylate synthetase family: unique interferon-inducible enzymes catalyzing 2′-5′ instead of 3′-5′ phosphodiester bond formation. Biochimie 89:779–788. doi:10.1016/j.biochi.2007.02.003

Hsieh JC, Wu C, Chung AE (1994) The binding of fibronectin to entactin is mediated through the 29 kDa amino terminal fragment of fibronectin and the G2 domain of entactin. Biochem Biophys Res Commun 199:1509–1517. doi:10.1006/bbrc.1994.1402

ISO (2008) Particle size analysis — dynamic light scattering (DLS), 22412 International Standards Organization. https://www.iso.org/obp/ui/ - iso:std:iso:22412:en. Accessed July 2016

Jakeman E, Pike ER (1969) Spectrum of clipped photon-counting fluctuations of gaussian light. J Phys Part Gen 2:411. doi:10.1088/0305-4470/2/3/021

Jamieson AM, Downs CE, Walton AG (1972) Studies of elastin coacervation by quasielastic light scattering. Biochim Biophys Acta 271: 34–47. doi:10.1016/0005-2795(72)90130-4

Khan AA, Bose C, Yam LS, Soloski MJ, Rupp F (2001) Physiological regulation of the immunological synapse by agrin. Science 292: 1681–1686. doi:10.1126/science.1056594

Kim I, McKenna SA, Viani Puglisi E, Puglisi JD (2007) Rapid purification of RNAs using fast performance liquid chromatography (FPLC). RNA 13:289–294. doi:10.1261/rna.342607

Koppel DE (1972) Analysis of macromolecular polydispersity in intensity correlation spectroscopy: the method of cumulants. J Chem Phys 57:4814. doi:10.1063/1.1678153

Kuratomi Y, Nomizu M, Tanaka K, Ponce ML, Komiyama S, Kleinman HK, Yamada Y (2002) Laminin gamma 1 chain peptide, C-16 (KAFDITYVRLKF), promotes migration, MMP-9 secretion, and pulmonary metastasis of B16-F10 mouse melanoma cells. Br J Cancer 86:1169–1173. doi:10.1038/sj.bjc.6600187

Landau LD, Placzek G (1934).Struktur der unverschobenen Streulinie. Z Phys Sowjetunion 5:172–173

Livesey AK, Licinio P, Delaye M (1986) Maximum entropy analysis of quasielastic light scattering from colloidal dispersions. J Chem Phys 84:5102–5107. doi:10.1063/1.450663

Lorber B, Fischer F, Bailly M, Roy H, Kern D (2012) Protein analysis by dynamic light scattering: methods and techniques for students. Biochem Mol Biol Educ 40:372–382. doi:10.1002/bmb.20644

Malvern Instruments (2014) TN101104 Intensity Volume Number. Malvern Instruments Limited. http://www.malvern.com/en/pdf/secure/TN101104IntensityVolumeNumber.pdf. Accessed July 2016

Mascarenhas JB, Ruegg MA, Winzen U, Halfter W, Engel J, Stetefeld J (2003) Mapping of the laminin-binding site of the N-terminal agrin domain (NtA). EMBO J 22:529–536. doi:10.1093/emboj/cdg041

Mayer U et al (1993) A single EGF-like motif of laminin is responsible for high affinity nidogen binding. EMBO J 12:1879–1885

McKenna SA, Lindhout DA, Shimoike T, Puglisi JD (2007) Biophysical and biochemical investigations of dsRNA-activated kinase PKR. Methods Enzymol 430:373–396. doi:10.1016/S0076-6879(07)30014-1

Meier M et al (2013) Binding of G-quadruplexes to the N-terminal recognition domain of the RNA helicase associated with AU-rich element (RHAU). J Biol Chem 288:35014–35027. doi:10.1074/jbc.M113.512970

Meng H, Deo S, Xiong S, Dzananovic E, Donald LJ, van Dijk CW, McKenna SA (2012) Regulation of the interferon-inducible 2′-5′-oligoadenylate synthetases by adenovirus VA(I) RNA. J Mol Biol 422:635–649. doi:10.1016/j.jmb.2012.06.017

Mie G (1908) Beiträge zur Optik trüber Medien, speziell kolloidaler Metallösungen. Ann Phys 330:377–445. doi:10.1002/andp.19083300302

Morrison ID, Grabowski EF, Herb CA (1985). Improved techniques for particle size determination by quasi-elastic light scattering. Langmuir 1:496–501 doi:10.1021/la00064a016

Nieuwenhuysen P, Clauwaert J (1981) Quasi-elastic light scattering of Artemia ribosomes sedimented in a CsCl density gradient. J Biochem Biophys Methods 5:279–286

Nitkin RM, Smith MA, Magill C, Fallon JR, Yao YM, Wallace BG, McMahan UJ (1987) Identification of agrin, a synaptic organizing protein from Torpedo electric organ. J Cell Biol 105:2471–2478

Nobbmann U et al (2007) Dynamic light scattering as a relative tool for assessing the molecular integrity and stability of monoclonal antibodies. Biotechnol Genet Eng Rev 24:117–128. doi:10.1080/02648725.2007.10648095

Nyeo SL, Chu B (1989). Maximum-entropy analysis of photon correlation spectroscopy data. Macromolecules 22:3998–4009 doi:10.1021/ma00200a031

Ortega A, Amoros D, Garcia de la Torre J (2011). Global fit and structure optimization of flexible and rigid macromolecules and nanoparticles from analytical ultracentrifugation and other dilute solution properties. Methods 54:115–123. doi:10.1016/j.ymeth.2010.12.004

Ortega A, Amoros D, Garcia de la Torre J (2011a) Prediction of hydrodynamic and other solution properties of rigid proteins from atomic- and residue-level models. Biophys J 101:892–898. doi:10.1016/j.bpj.2011.06.046

Ortega A, Garcia de la Torre J (2007) Equivalent radii and ratios of radii from solution properties as indicators of macromolecular conformation, shape, and flexibility. Biomacromolecules 8:2464–2475. doi:10.1021/bm700473f

Ostrowsky N, Sornette D, Parker P, Pike ER (1981) Exponential sampling method for light scattering polydispersity analysis. Opt Acta 28:1059–1070

Patel TR, Bernards C, Meier M, McEleney K, Winzor DJ, Koch M, Stetefeld J (2014) Structural elucidation of full-length nidogen and the laminin–nidogen complex in solution. Matrix Biol 33:60–67. doi:10.1016/j.matbio.2013.07.009

Patel TR, Meier M, Li J, Morris G, Rowe AJ, Stetefeld J (2011) T-shaped arrangement of the recombinant agrin G3-IgG Fc protein. Protein Sci 20:931–940. doi:10.1002/pro.628

Patel TR et al (2010) Nano-structure of the laminin gamma-1 short arm reveals an extended and curved multidomain assembly. Matrix Biol 29:565–572. doi:10.1016/j.matbio.2010.07.004

Patel TR, Reuten R, Xiong S, Meier M, Winzor DJ, Koch M, Stetefeld J (2012) Determination of a molecular shape for netrin-4 from hydrodynamic and small angle X-ray scattering measurements. Matrix Biol 31:135–140. doi:10.1016/j.matbio.2011.11.004

Pecora R (1964) Doppler shifts in light scattering from pure liquids and polymer solutions. J Chem Phys 40:1604. doi:10.1063/1.1725368

Pecora R (1972) Quasi-elastic light scattering from macromolecules. Annu Rev Biophys Bioeng 1:257–276. doi:10.1146/annurev.bb.01.060172.001353

Pike ER (1972) The accuracy of diffusion-constant measurements by digital autocorrelation of photon-counting fluctuations. Journal de Physique Colloques 33:C1-177–C171-180. doi:10.1051/jphyscol:1972132

Provencher SW (1982a) A constrained regularization method for inverting data represented by linear algebraic or integral equations. Comput Phys Commun 27:213–227. doi:10.1016/0010-4655(82)90173-4

Provencher SW (1982b) CONTIN: A general purpose constrained regularization programm for inverting noisy linear algebraic and integral equations. Comput Phys Commun 27:229–242. doi:10.1016/0010-4655(82)90174-6

Provencher SW, Stepanek P (1996) Global analysis of dynamic light scattering autocorrelation functions. Part Part Syst Char 13:291–294. doi:10.1002/ppsc.19960130507

Pusey PN (1972) Correlation and light beating spectroscopy. In: Cummings HZ, Pike ER (eds) Photon correlation and light beating spectroscopy, Plenum, New York, pp 387–428

Pyun JA, Cha DH, Kwack K (2012) LAMC1 gene is associated with premature ovarian failure. Maturitas 71:402–406. doi:10.1016/j.maturitas.2012.01.011

Raltson G (1993) Introduction to analytical ultracentrifugation. Beckman Instruments, Inc., Fullerton CA

Rimai L, Hichmott JT Jr, Carew EB, Cole T (1970) Quasi-elastic light scattering by diffusional fluctuations in RNase solutions. Biophys J 10:20–37. doi:10.1016/S0006-3495(70)86283-X

Sasaki T, Gohring W, Pan TC, Chu ML, Timpl R (1995a) Binding of mouse and human fibulin-2 to extracellular matrix ligands. J Mol Biol 254:892–899. doi:10.1006/jmbi.1995.0664

Sasaki T, Kostka G, Gohring W, Wiedemann H, Mann K, Chu ML, Timpl R (1995b) Structural characterization of two variants of fibulin-1 that differ in nidogen affinity. J Mol Biol 245:241–250

Schneiders FI et al (2007) Binding of netrin-4 to laminin short arms regulates basement membrane assembly. J Biol Chem 282:23750–23758. doi:10.1074/jbc.M703137200

Schurr JM (1977) Dynamic light scattering of biopolymers and biocolloids. CRC Crit Rev Biochem 4:371–431. doi:10.3109/10409237709105461

Scott DJ, Patel TR, Besong DMT, Stetefeld J, Winzor DJ (2011) Examination of the discrepancy between size estimates for ovalbumin from small-angle X-ray scattering and other physicochemical measurements. J Phys Chem B 115:10725–10729. doi:10.1021/jp2006149

Serdyuk IN, Zaccai NR, Zaccai J (2007) Methods in Molecular Biophysics : Structure, Dynamics, Function. Cambridge University Press, Cambridge

Siegert AJF (1949) On the fluctuations in signals returned by many independently moving scatterers. Massachusetts Institute of Technology, Radiation Laboratory Report, 465. MIT, Cambridge

Stetefeld J et al (2004) Modulation of agrin function by alternative splicing and Ca2+ binding. Structure 12:503–515. doi:10.1016/j.str.2004.02.001

Stetefeld J et al (2001) The laminin-binding domain of agrin is structurally related to N-TIMP-1. Nat Struct Biol 8:705–709. doi:10.1038/90422

Stokes GG (1845) On the theories of internal friction of fluids in motion. Trans Cam Philos Soc 8:287–305

Strutt JW (1871a) LVIII. On the scattering of light by small particles. Philos Mag Ser 4(41):447–454. doi:10.1080/14786447108640507

Strutt JW (1871b) XXXVI. On the light from the sky, its polarization and colour. Philos Mag Ser 4(41):274–279. doi:10.1080/14786447108640479

Sutherland W (1905) LXXV. A dynamical theory of diffusion for non-electrolytes and the molecular mass of albumin. Philos Mag Ser 6(9):781–785. doi:10.1080/14786440509463331

Svedberg T, Pedersen KO (1940) The ultracentrifuge. Oxford University Press, Oxford

Tanford C (1961) Physical chemistry of macromolecules. John Wiley & Sons, Inc., New York. doi:10.1002/jps.2600510233

Tyndall J (1868). On the Blue Colour of the Sky, the Polarization of Skylight, and on the Polarization of Light by Cloudy Matter Generally. Proceedings of the Royal Society of London 17:223–233 doi:10.1098/rspl.1868.0033

v. Smoluchowski M (1908).Molekular-kinetische Theorie der Opaleszenz von Gasen im kritischen Zustande, sowie einiger verwandter Erscheinungen. Annalen der Physik 330:205–226 doi:10.1002/andp.19083300203

Vadlamani G et al (2015) The beta-lactamase gene regulator AmpR is a tetramer that recognizes and binds the D-Ala-D-Ala motif of its repressor UDP-N-acetylmuramic acid (MurNAc)-pentapeptide. J Biol Chem 290:2630–2643. doi:10.1074/jbc.M114.618199

Van Holde KE (1970) Physical characterization of the protein molecule. Mol Biol Biochem Biophys 8:2–24

Wyatt PJ (1993) Light scattering and the absolute characterization of macromolecules. Anal Chim Acta 272:1–40. doi:10.1016/0003-2670(93)80373-S

Zakharov P, Scheffold F (2009) Advances in dynamic light scattering techniques. In: Kokhanovsky A (ed) Light scattering reviews 4: single light scattering and radiative transfer. Springer, Berlin Heidelberg, pp 433–467. 10.1007/978-3-540-74276-0_8

Zimm BH (1945) Molecular theory of the scattering of light in fluids. J Chem Phys 13:141–145. doi:10.1063/1.1724013

Zimm BH (1948) Apparatus and methods for measurement and interpretation of the angular variation of light scattering; preliminary results on polystyrene solutions. J Chem Phys 16:1099–1116. doi:10.1063/1.1746740